Optical properties of strained antimonide-based heterostructures

M. Dinu, J. E. Cunningham, F. Quochi, and J. Shah

Citation: Journal of Applied Physics **94**, 1506 (2003); doi: 10.1063/1.1583147
View online: http://dx.doi.org/10.1063/1.1583147
View Table of Contents: http://scitation.aip.org/content/aip/journal/jap/94/3?ver=pdfcov
Published by the AIP Publishing

Optical properties of strained antimonide-based heterostructures

M. Dinu,[a] J. E. Cunningham, F. Quochi, and J. Shah
Bell Laboratories, Lucent Technologies, 101 Crawfords Corner Road, Holmdel, New Jersey 07733

(Received 7 March 2003; accepted 28 April 2003)

The optical properties of strained GaAsSb/GaAs quantum wells grown by molecular beam epitaxy were investigated by photoluminescence spectroscopy as a function of excitation intensity and temperature. Photoluminescence spectra exhibit strong blue shifts of the emission peak with increasing excitation intensity, ascribed to the interplay between band tail filling at low carrier densities and electrostatic band bending at high carrier concentrations. Spectroscopic data are consistent with a type II band alignment, with a small conduction band offset ($\Delta E_c \sim 100$ meV), and gain spectra are blue shifted with respect to the low excitation luminescence. The large material gain and fast carrier recombination lifetimes demonstrate the viability of this material system for the fabrication of 1.3 μm lasers. © *2003 American Institute of Physics.* [DOI: 10.1063/1.1583147]

I. INTRODUCTION

$GaAs_{1-x}Sb_x$ quantum wells (QWs) grown on GaAs substrates, with an antimony fraction of approximately 30%, emit at wavelengths near 1.3 μm. This material system has attracted considerable interest recently because of the possibility of manufacturing monolithic vertical cavity surface emitting lasers (VCSELs) on gallium arsenide substrates.[1–4] Monolithically grown VCSELs operating near 1.3 μm would constitute an attractive cost-effective solution for transmitters in the metro telecommunications market. Nevertheless, a long-standing problem for the fabrication of high efficiency devices in this wavelength range is the growth of high-gain active material (conventionally, in the InGaAsP material system) on high contrast mirrors, which make use of AlAs/GaAs reflectors grown on GaAs substrates. Existing VCSELs operating in this spectral region include wafer fused devices with conventional InGaAsP active regions.[5] A different approach makes use of monolithic VCSELs with nonconventional gain materials grown on GaAs substrates: recent developments include InGaAs quantum dots,[6] InGaAsN quantum wells,[7] and GaAsSb quantum wells.[1–4] The properties of these active materials is a subject of ongoing study.

Previous realizations of antimonide-based quantum well devices include molecular-beam epitaxy (MBE) -grown edge emitters up to 1.30 μm (Refs. 8 and 9) and VCSELs operating cw at 1.23 μm (Ref. 2) and 1.30 μm,[4] as well as low-threshold metal–oxide chemical vapor deposition (MOCVD)-grown edge-emitters at 1.19 μm.[10] In spite of the significance of these advances, many material and optical properties of the GaAsSb/GaAs material system are not well understood. For instance, the band alignment and the band offsets of this highly strained material system are not definitely established.[11] A type II or spatially staggered alignment has generally been proposed for the GaAsSb/GaAs interface,[12,13] with electrons confined in the GaAs layer and holes confined in GaAsSb. However, some workers claim a type I band alignment for the low antimony fraction alloy ($x_{Sb}=0.1-0.3$).[14,15] For the high antimony fraction interface (GaSb/GaAs), model-solid theory[16,17] predicts a type II alignment with a conduction band discontinuity $\Delta E_c = -640$ meV and a valence band offset ratio $Q_v = \Delta E_v/(\Delta E_v + \Delta E_c) = 2.75$ when taking into account strain. However, experimental data,[16,18] to be discussed further, indicate a smaller value $Q_v \sim 1.15$. For low Sb fraction alloys, the literature reports larger offset values, such as $Q_v = 1.7$ for $GaAs_{0.90}Sb_{0.10}/GaAs$ (Ref. 13) and $Q_v = 2.2$ for $GaAs_{0.73}Sb_{0.27}/GaAs$.[12] Detailed knowledge of the band offsets is especially important for type II lasers, since the gain tends to be smaller than in type I lasers[19] and the electron–hole wave-function overlap has to be carefully optimized.[20] The origin of the luminescence and gain properties of GaAsSb/GaAs quantum wells is another issue of discussion.[11] The occurrence of the photoluminescence at wavelengths roughly equal to the unstrained GaAsSb band gap is sometimes cited as evidence for strain relaxation or intermixing[1] or for the formation of quantum dots,[11] although x-ray and other structural studies[21] typically confirm the formation of a pseudomorphic two-dimensional antimonide layer.

Here, we present detailed studies of GaAsSb/GaAs quantum well photoluminescence as a function of temperature and excitation power, as well as room-temperature experimental results on optical properties relevant to laser function. We also discuss the nature of the band line-up in the GaAsSb/GaAs material system and its significance for antimonide quantum wells as emitting materials.

II. PHOTOLUMINESCENCE STUDIES

The samples studied here were grown by gas-source molecular-beam epitaxy using arsine and solid source antimony and were characterized using x-ray diffraction to determine the Sb concentration in the quantum wells. Secondary ion mass spectroscopy (SIMS) was used to assess the degree of localization of Sb. The well widths are below the critical thickness, which for antimony fractions around $x_{Sb} \sim 0.30$ and 2.3% strain is approximately equal to 70 Å, and

[a]Electronic mail: mdinu@lucent.com

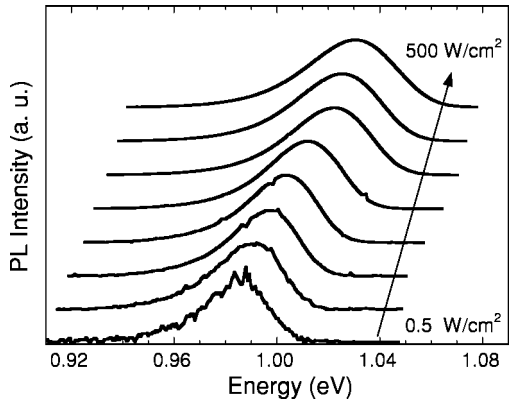

FIG. 1. Photoluminescence of a $GaAs_{0.7}Sb_{0.3}/GaAs$ single quantum well for a series of excitation intensities, at low temperature ($T=9$ K). The curves are normalized to unity and offset for clarity. The excitation intensity varies in the range $I_{exc}=0.5$-500 W/cm^2.

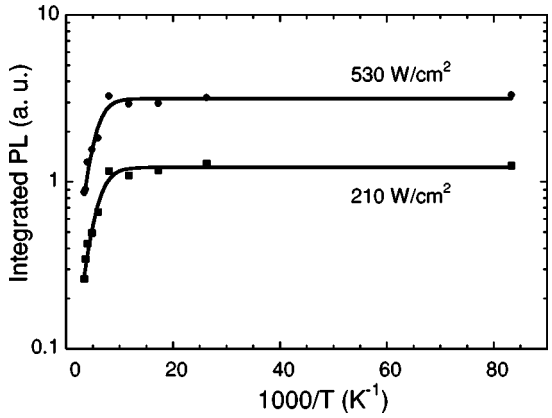

FIG. 3. Spectrally integrated photoluminescence as a function of temperature for a GaAsSb/GaAs single quantum well for two excitation conditions. The solid lines correspond to a thermally activated carrier escape model.

two-dimensional growth was ensured *in situ* using reflection high-energy electron diffraction (RHEED) spectroscopy.[21] Further growth and structural details can be found in Ref. 21.

Photoluminescence (PL) measurements were performed as a function of temperature over three orders of magnitude of excitation power using a helium–neon laser ($\lambda=633$ nm), focused to a 50 μm spot, as the excitation source. The sample consisted of a single 60 Å $GaAs_{1-x}Sb_x$ quantum well ($x\sim0.33$), grown on a GaAs substrate and a 0.5 μm GaAs buffer layer; the quantum well was capped by a 1000 Å GaAs layer. The emission was measured at the output of a single-grating spectrometer using a Ge photodiode in conjunction with lock-in detection. Figure 1 shows the normalized spectra as a function of excitation power for the GaAsSb quantum well at liquid helium temperatures ($T=9$ K). The compressive strain increases the low-temperature band gap of the antimonide layer to ~1.16 eV, and the luminescence peak energy is roughly equal to the bandgap corresponding to the unstrained epilayer.

The photoluminescence peak exhibits pronounced blueshifts as a function of excitation intensity, of 45 meV over the range of intensities shown in Fig. 2. The low-intensity lineshape is fairly broad, with a full width at half maximum (FWHM) of approximately 28 meV. With increasing excitation intensity, the photoluminescence linewidth increases to 42 meV. The large low-excitation linewidth is likely due to inhomogeneous broadening caused by alloy fluctuations, which are expected to occur due to the segregation of the more weakly bound Sb at the GaAsSb/GaAs interface.[22] Photoluminescence blue shifts with increasing power are typically attributed either to band filling of localized states (as, for example, in InGaN/GaN quantum wells, where stimulated emission occurs from the localized states[23]), or to electrostatic band bending due to charge separation in type II heterostructures. Band filling of a distribution of localized states is also consistent with linewidth broadening with increasing excitation.

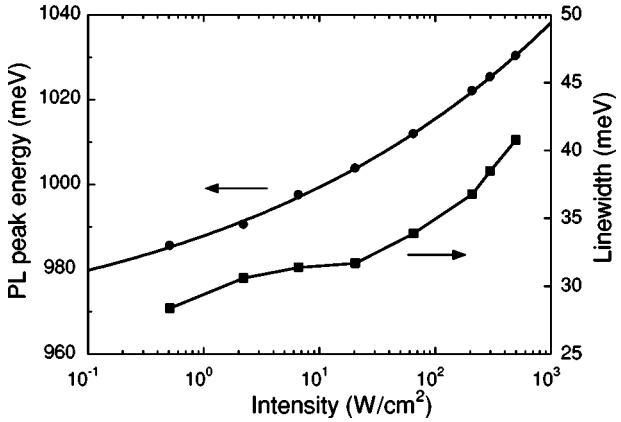

FIG. 2. Photoluminescence peak energy and photoluminescence linewidth vs excitation power for a $GaAs_{1-x}Sb_x/GaAs$ ($x\sim0.33$) single quantum well at $T=9$ K. The solid lines are plotted to guide the eye.

To elucidate the origin of the photoluminescence peak blueshifts with increasing excitation, we have performed detailed studies of the luminescence as a function of temperature. Figure 3 shows the dependence of the spectrally integrated photoluminescence intensity on temperature for two representative excitation conditions. The solid lines are fits to the data using a model for thermally activated carrier escape.[24,25] Remarkably, the PL intensity decreases by only a factor of 5 from low temperature ($T=9$ K) to room temperature, which is indicative of high quality quantum wells, with a low density of nonradiative defects. The Arrhenius dependence at high temperatures corresponds to an activation (escape) energy of approximately 23 meV.

The dependence of the photoluminescence spectra on temperature for a fixed excitation power $I_{exc}=500$ W/cm^2 is shown in Fig. 4. The linewidth of the PL spectra increases monotonically with temperature, as shown in Fig. 5. The inflection point in the linewidth near $T=50$ K suggests a transition to a different regime, where the linewidth is dominated by thermal activation of carriers from band tail states. Also plotted in Fig. 5 are the exponential slopes of the low- and high-energy sides of the PL spectrum E_{sl}, extracted by fitting the leading and trailing edges of the spectra in Fig. 4 with the dependence $I_{PL}(E)\propto\exp(\pm E/E_{sl})$, respectively. The exponential slope of the high-energy side of the photoluminescence spectrum increases with increasing temperature and is equal to kT within experimental error, indicating a thermal

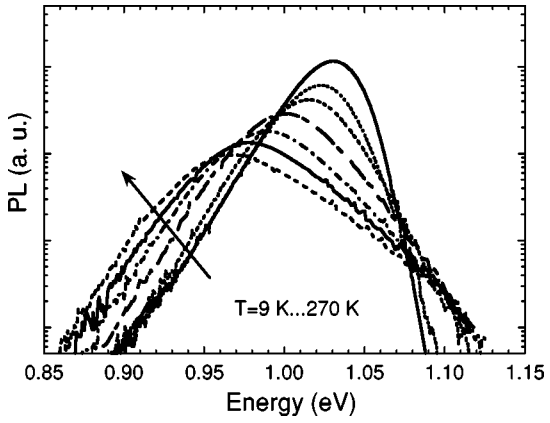

FIG. 4. Photoluminescence spectra as a function of temperature for a GaAsSb/GaAs single quantum well for $I_{exc}=500$ W/cm^2 for several temperature values. The temperature increases in the direction shown by the arrow, and spectra are taken for $T=9$, 60, 105, 150, 190, 240, and 270 K.

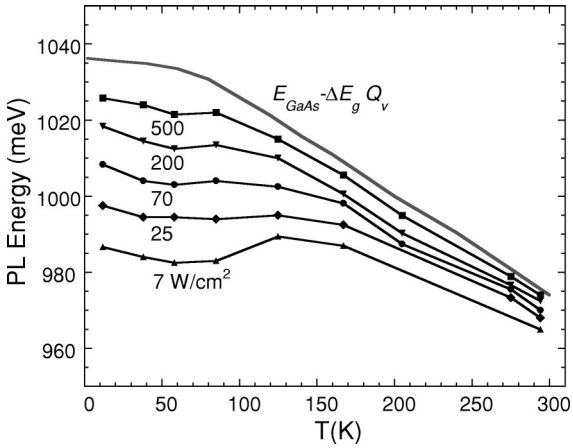

FIG. 6. Photoluminescence peak energy vs temperature for a GaAsSb/GaAs single quantum well for various excitation conditions. The points are experimental data, and the solid curve is the Varshni-like temperature dependence of the type II transition.

(Boltzmann) distribution for the carrier population. The low-energy slope of the spectrum is independent of temperature, and thus can be attributed to an exponential tail of localized states, due possibly to potential fluctuations. We can estimate the potential fluctuations by fitting the low-energy tail of the PL spectrum with a density of states of the form $g(E)\propto 1+\tanh[(E-E_0)/\delta E]$, where E_0 is the center and δE is the width of the distribution. In this approximation, δE is $\sim$1.54 times the low-energy PL spectrum exponential slope. The potential fluctuations then are of the order of $\delta E \sim 22.7$ meV for this sample. This type of distribution of band tail states is not uncommon in ternary or quaternary materials, especially in highly strained materials.[23]

The PL peak energy versus temperature is plotted in Fig. 6 for a range of excitation intensities. In the low excitation regime, the PL peaks exhibit red shifts with increasing temperature up to $T=60$ K, then the PL peak energy increases with temperature between 60 and 120 K, after which it monotonically decreases with increasing temperature. Thus, the PL peak exhibits a characteristic ''S'' shape with increasing temperature, usually attributed to competition between radiative and nonradiative recombination processes and thermal activation from the band tail states.[23] The solid line designates the Varshni-like temperature dependence of the energy of the type II transition, calculated using known band parameters and temperature coefficients for GaAs and GaAsSb. The band offset ratio Q_v we have used in deriving the solid curve is discussed in the following paragraphs. At high excitations, the deviation from the Varshni dependence of the interband transition energy $E(T)=E_{0\,\mathrm{K}}-AT^2/(B+T)$ is less pronounced. Therefore, we can conclude that for temperatures above $\sim$120 K or for high excitation conditions the band tail states are occupied either with a thermalized carrier distribution or with a population of photoexcited carriers.

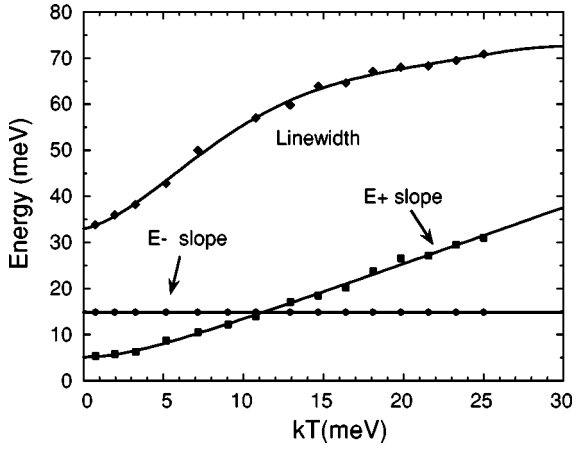

FIG. 5. Photoluminescence linewidth and positive and negative exponential slopes of the photoluminescence spectrum vs temperature.

The nonmonotonic dependence of the PL peak energy with temperature, the blue shifts of the luminescence peak with increasing excitation power, and the exponential tail of the PL spectrum all point to the existence of a distribution of localized states with a localization energy of around 23 meV. These states become thermally activated at temperatures above $\sim$100 K, where a crossover occurs to ''intrinsic'' quantum well luminescence.

The blue shifts of luminescence peaks as a function of excitation power are usually considered evidence for a type II band alignment, most commonly assumed for the GaSb/GaAs interface. Because the distribution of localized band tail states gives rise to qualitatively similar trend, we resort to an alternative approach of determining the band alignment, which relies on absolute comparisons between calculated and measured transition energies.

Figure 7 shows the calculated transition energy for (wide) GaAsSb/GaAs quantum wells, as a function of Sb fraction and valence band offset ratio Q_v. We have used known band-gap parameters and deformation potentials for GaAs and GaAsSb (Refs. 26 and 27) and neglected any exciton binding energies or carrier confinement energies. The symbols denote experimental values from this work and values extracted from data previously published in the literature, and are plotted on the respective equal energy curves for the corresponding Sb fraction. All transition energy values have

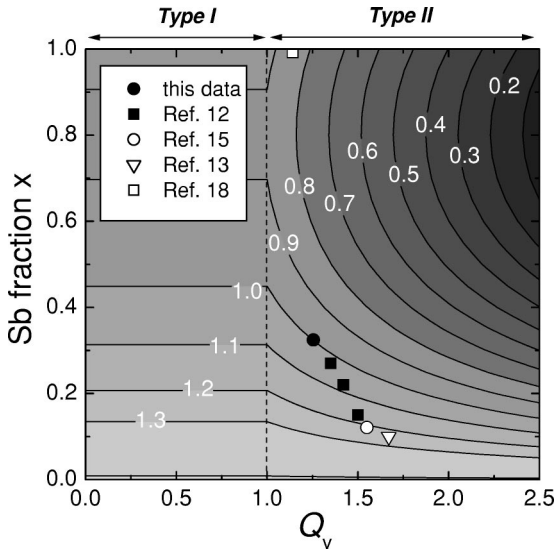

FIG. 7. Contour plots of the transition energies as a function of valence band offset and Sb fraction. Wide GaAsSb quantum wells have been assumed. The energy values corresponding to the equal energy curves are shown in white. The points are experimental data from this work and the literature.

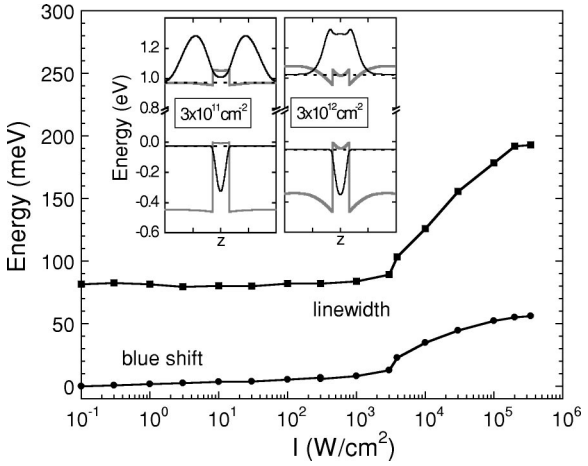

FIG. 8. Photoluminescence peak energy and photoluminescence linewidth vs excitation power for a $GaAs_{0.7}Sb_{0.3}$/GaAs single quantum well. Inset: schematic band edge profile (thick solid lines) and heavy hole and electron probability densities (solid lines) calculated for carrier sheet densities $\sigma = 3\times10^{11}$ cm^{-2} and $\sigma = 3\times10^{12}$ cm^{-2}.

been scaled to room temperature. An important observation to be extracted from Fig. 7 is that, in the limit of wide wells, a type I band alignment is insensitive to the valence band offset between the strained GaAsSb well and the GaAs barriers. This is obviously due to the fact that only the quantum confinement energy of the electrons and the holes confined in the well is sensitive to the band offset, and furthermore this dependence is weak if the confinement potential is large (deep wells). On the contrary, for type II band alignments, the transition energy $E = E_{\mathrm{GaAs}} - Q_v \Delta E_g$ is strongly dependent on the valence band offset Q_v, and only weakly dependent on the small confinement energy of the carriers (heavy holes in this case), even for narrow wells. The valence band offset can then be easily determined if the difference between the GaAs band gap and the band gap of the strained layer is known. We estimate that the approximations used in the calculations are in error by no more than ~10 meV for type II wells, and furthermore the transition energies are always underestimated by neglecting confinement energies; in the type II region of the parameter space, this would lead in fact to a slight underestimate of the offset Q_v.

The graphical representation in Fig. 7 indicates that the valence band offset near $x_{\mathrm{Sb}} = 0.33$ is $Q_v = 1.25$, which results in a small conduction band offset $\Delta E_c = 100$ meV. Interestingly, the plotted points for the range of values compiled from the literature suggests a band offset dependent on the antimony fraction. Note that the valence band offset defined here refers to the *strained* interface between the two semiconductors, which is the experimentally relevant situation. Theoretical treatments of the band line-ups in the GaAsSb system such as the model-solid theory[17] or a more recent empirical model[19] assume that the valence band edge or the conduction band edge, respectively, of the unstrained interface are not bowed. Both theories predict a value Q_v ~2.75 for the strained GaSb/GaAs interface, which is in conflict with experimental points for quantum wells with high Sb fraction ($x_{\mathrm{Sb}} \sim 1.0$). This implies that, similar to the bandgap of GaAsSb, the valence band offset ratio Q_v of the GaAsSb/GaAs interface also has a large bowing parameter. Clearly, further theoretical and experimental studies are necessary in order to elucidate the band line-up at the strained GaAsSb/GaAs interface.

III. ROOM-TEMPERATURE OPTICAL PROPERTIES

In order to study the properties of the antimonide quantum wells relevant for their use as laser emitters, room-temperature measurements were performed on quantum well samples consisting of a single 60 Å GaAsSb quantum well ($x_{\mathrm{Sb}} \sim 0.35$) surrounded by 3000 Å of GaAs and embedded in a $Al_{0.35}Ga_{0.65}As$ waveguide cladding. Photoluminescence experiments used a cw Ti:sapphire laser source ($\lambda = 830$ nm) focused to a 50 μm spot; for higher pump intensities the pump beam was modulated into 1 μs pulses in order to avoid heating.

Figure 8 shows the energy peak of the photoluminescence as a function of excitation intensity. With increasing excitation density, the peak of the photoluminescence exhibits pronounced blue shifts, accompanied by an increase in linewidth due to Fermi filling, as shown in Fig. 2. Two intensity regimes can be distinguished. Below 10^3 W/cm^2, the blue shifts follow a weak power-law dependence on the intensity (with an exponent $\alpha = 0.16$), and the linewidth remains roughly constant. The total blue shift in this intensity range is 9 meV. Between 10^3 and 10^5 W/cm^2, the PL peak blueshifts by 45 meV.

Based on the discussion in the previous section, we attribute the blue shifts in the low-intensity regime at least partially to band filling of band tail states, and the blue shift of the peak position at high powers to electrostatic band bending due to the spatial separation of the electrons and the holes in a type II quantum well. Further support for this assignment is given by the onset of the large blue shift re-

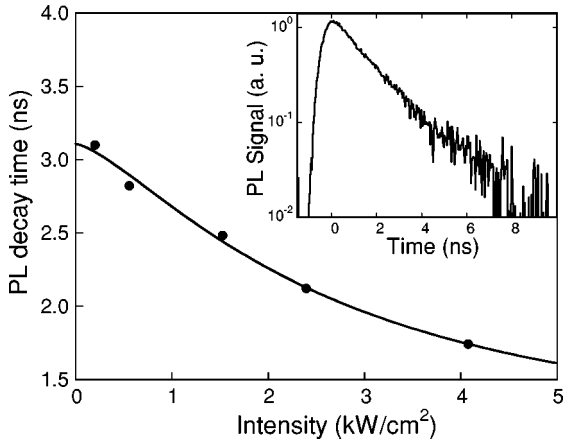

FIG. 9. Photoluminescence decay time at room temperature vs average excitation intensity. The inset shows the PL decay curve for $I_{exc} = 4.1$ kW/cm^2.

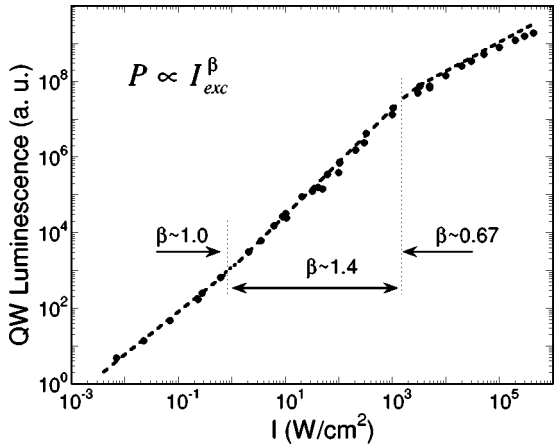

FIG. 10. Integrated quantum well luminescence over eight decades of excitation intensity at room temperature. The lines represent the power law dependences indicated on the plot.

gime at intensities of the order of 10^3 W/cm^2. At this intensity range the type II quantum wells evolve from a flat band situation, illustrated in the left inset in Fig. 8, to a strongly band bending situation (right inset), where the wave-function overlap of the electrons and the holes, initially confined in separate layers, approaches values near unity. Using an electrostatic band bending model in the envelope function approximation, where the Schrödinger and Poisson equations are solved iteratively in a self-consistent manner,[20] the carrier sheet concentration for the onset of significant wavefunction overlap and blue shifts is derived as $\sigma \sim 10^{12}$ cm^{-2}. It is interesting to note that GaSb (and presumably its alloys) are slightly *p*-type as grown,[28] which may lead to a small initial band bending due to residual doping in the range $\sigma \sim 10^8 - 10^9$ cm^{-2}.

In order to determine the carrier lifetime as a function of carrier density, photoluminescence lifetime measurements were performed using an ultrafast Ti:sapphire laser pump (100 fs pulses, 76 MHz repetition rate), and a fast amplified InGaAs photodiode, whose output was detected using a fast oscilloscope. The temporal resolution of this detection scheme was 0.60 ns (FWHM). The PL decay time is plotted in Fig. 9 as a function of average excitation intensity. The inset shows the decay of the PL signal for a value of the excitation intensity $I_{exc} = 4.1$ kW/cm^2. The PL lifetime is $\tau \sim 3.1$ ns at the lowest pump power, equivalent to an injected carrier density $\sigma \approx 10^{12}$ cm^{-2}. Using the measured photoluminescence lifetime values, we obtain an estimate for the sheet carrier density at $I_{exc} = 1$ kW/cm^2, yielding $\sigma \sim 10^{12}$ cm^{-2}. Therefore, the transition in Fig. 8 occurs in the expected range for the onset of blue shifts. We estimate that the band tail states are 95% filled for this density, therefore, the blue shift originates mainly from band bending due to extended states.

The dependence of the integrated photoluminescence on cw excitation intensity was measured in a range of excitation intensities of over eight orders of magnitude, and the experimental results are shown in Fig. 10. Three intensity regimes can be distinguished. At low intensities, the PL depends linearly on excitation. At intermediate intensities, the dependence follows a power law with the exponent $\beta \sim 1.4$, and at high intensities $\beta \sim 0.67$. The latter exponent is close to the 2/3 value suggesting the onset of Auger recombination at the higher carrier concentrations. Auger recombination can be an important loss mechanism for high threshold lasers, such as type II lasers, where electrostatic band bending is necessary in order to achieve wave-function overlap to increase dipole moments from their low flat band values, a prerequisite for achieving net gain. On the other hand, it is difficult to attribute the low excitation power law dependences to any particular recombination mechanism. However, superunitary exponents near $\beta = 1.5$ have generally been ascribed to recombination on a population of partially filled traps,[29] while intrinsic electron-hole recombination leads to a linear intensity dependence. In the case of the antimonide quantum wells, several competing recombination mechanisms may play a role at low powers.

A type II alignment in the GaAsSb/GaAs quantum wells is further supported by absorption measurements on multiple quantum well (MQW) samples. The samples consisted of six 50 Å $GaAs_{0.7}Sb_{0.3}$ quantum wells grown on a GaAs substrate, separated by 500 Å barriers and capped by a 1000 Å GaAs layer. The transmission was measured using a white-light source (tungsten lamp) and a spectrometer fitted with an infrared detector array. Figure 11 shows the room-temperature absorbance, defined as $A = \ln(1/T)$, where T is the transmission corrected for Fresnel reflections at the semiconductor–air interfaces. In order to separate the contribution of the substrate, the absorbance of the bare GaAs substrate with the quantum wells etched off was subtracted from the data. The absorbance spectrum is essentially featureless, with a slow increase at energies larger than the photoluminescence peak, as expected for type II quantum wells. No well-defined spectral features, such as the step increase in absorption characteristic of type I quantum wells, occur near the emission wavelength. To the contrary, the absorbance seems to go through a minimum near the emission wavelength. Although it is difficult to put an exact value on the upper limit for the absorbance, the absorbance per well at the emission wavelength is smaller than approximately 2

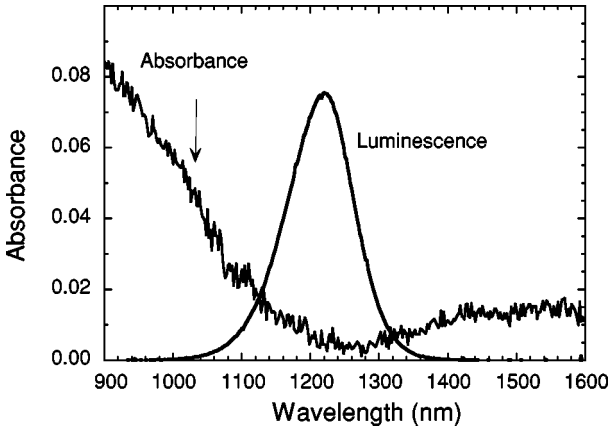

FIG. 11. Absorbance of a $GaAs_{0.7}Sb_{0.3}/GaAs$ multiple quantum well sample (six quantum wells) and the photoluminescence spectrum corresponding to an excitation intensity $I_{exc}=500$ W/cm^2.

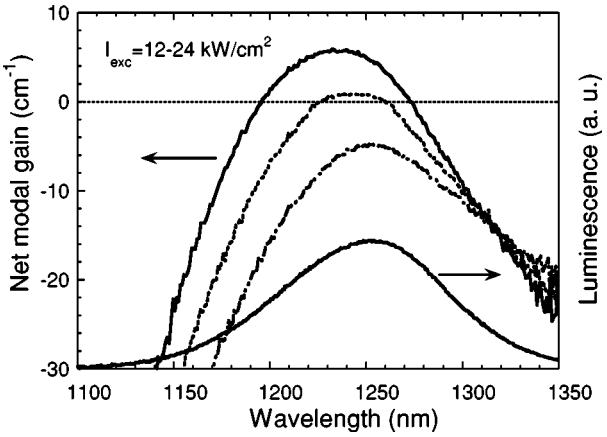

FIG. 12. Modal gain of the $GaAs_{0.7}Sb_{0.3}/GaAs$ waveguide sample. The peak pump intensity values were 12, 18, and 24 kW/cm^2. The low-excitation PL spectrum is also shown.

$\times 10^{-3}$. This is consistent with the absorption per well (1.3×10^{-3}, or $\alpha = 2600$ cm^{-1} for a 50 Å well) estimated from the decrease in reflectivity near the cavity resonance as a function of the number of wells in a series of half-VCSEL cavities, and is smaller than that for type I quantum wells.[30] The small value of the absorption coefficient is due to the type II alignment, which gives small electron-hole overlap under flat band conditions, and also to the smaller transition matrix elements for lower bandgap materials. However, in type II quantum wells, the value of the absorption coefficient under flat band conditions bears little relationship to the maximum attainable gain, in contrast to type I wells.[31] Therefore, the value of the absorption does not in principle limit the attainable gain under strong pumping conditions, when the wavefunction overlap is large.

In order to evaluate the quantum well gain under high excitation conditions, we performed gain measurements on quantum well samples consisting of a single 60 Å quantum well surrounded by 3000 Å of GaAs and embedded in a $Al_{0.35}Ga_{0.65}$ As waveguide cladding. This structure has a confinement factor $\Gamma = 0.016$. The gain was measured using the variable stripe technique,[22] using a pulsed laser diode at 810 nm with 25 ns pulse width and 1.2 kHz repetition rate, focused to a 25 μm wide stripe 1 mm long. The repetition rate was kept small to avoid heating, and the pulse width was much longer than the radiative lifetime. The modal gain is defined as

$$g_m = \Gamma g - \alpha_i ,$$

where g is the material gain, Γ is the confinement factor, and α_i is the internal (background) absorption coefficient. The modal gain was determined from the stripe length dependence of the edge emission spectrum,

$$I_{PL} \propto [\exp(g_m L) - 1]/g_m ,$$

where L is the stripe length. The modal gain is plotted in Fig. 12, for three representative excitation intensities ($I_{exc}=12$, 18, and 24 kW/cm^2, respectively). The gain spectrum is blue shifted compared to the low-intensity luminescence, even when taking into account the inhomogeneous broadening. Assuming waveguide losses equal to $\alpha_i \sim 10$ cm^{-1}, the value of modal gain $g_m = 5.8$ cm^{-1} corresponds to a peak material gain as high as 990 cm^{-1} at 24 kW/cm^2 excitation intensity. Note, also, that this excitation intensity is much smaller than the excitation for which nonradiative Auger loss mechanisms start to become important, as shown in Fig. 10.

The pronounced inhomogeneous broadening of the wells, apparent from the PL spectrum in Fig. 12, is likely to reduce the material gain from its ideal value. The material gain of type II quantum wells also is expected to be smaller than for type I structures,[19,31] and reaching above-threshold conditions requires not only population inversion but also significant band bending to restore electron–hole wavefunction overlap and thus the transition dipole moment. However, several design strategies may be employed in order to reduce the threshold and optimize the gain of type II lasers. These include p-type doping of the quantum wells[8] and confinement of the electrons in adjacent quantum wells.[31] Therefore, the type II alignment is not necessarily detrimental to the suitability of antimonide quantum wells as efficient laser active media.

IV. CONCLUSIONS

In conclusion, photoluminescence studies of MBE-grown GaAsSb/GaAs quantum wells are consistent with a type II band alignment with a valence band offset $Q_v = 1.25$. We assign the blue shifts of the photoluminescence peaks with increasing intensity to the interplay between band filling of localized band tail states at low powers and electrostatic band bending under high excitation conditions. The room-temperature gain spectra are blue shifted relative to the low-excitation photoluminescence, and a net modal gain of 5.8 cm^{-1} is measured for a single quantum well device with an optical pump intensity of 24 kW/cm^2. Although the type II band alignment in this material system requires electrostatic band bending in order to achieve net gain, large material gain and short recombination lifetimes are achieved at carrier densities at which density-dependent nonradiative processes are negligible. These characteristics demonstrate the viability of this material system for the fabrication of 1.3 μm lasers.

[1] T. Anan, M. Yamada, K. Tokutome, S. Sugou, K. Nishi, and A. Kamei, Electron. Lett. **35**, 903 (1999).
[2] M. Yamada, T. Anan, K. Kurihara, K. Nishi, K. Tokutome, A. Kami, and S. Sugou, Electron. Lett. **36**, 637 (2000).
[3] F. Quochi, J. E. Cunningham, M. Dinu, and J. Shah, Electron. Lett. **36**, 2075 (2000).
[4] F. Quochi, D. C. Kilper, J. E. Cunningham, M. Dinu, and J. Shah, IEEE Photonics Technol. Lett. **13**, 921 (2001).
[5] J. Dudley, D. Babic, R. Mirin, L. Yang, B. Miller, R. Ram, T. Reynolds, E. Hu, and J. Bowers, Appl. Phys. Lett. **64**, 1463 (1994).
[6] J. A. Lott *et al.*, Electron. Lett. **36**, 1384 (2000).
[7] K. D. Choquette *et al.*, Electron. Lett. **36**, 1388 (2000).
[8] M. Yamada, T. Anan, K. Tokutome, A. Kamei, K. Nishi, and S. Sugou, IEEE Photonics Technol. Lett. **12**, 774 (2000).
[9] O. Blum and J. F. Klem, IEEE Photonics Technol. Lett. **12**, 771 (2000).
[10] S.-W. Ryu and P. D. Dapkus, Electron. Lett. **36**, 1387 (2000).
[11] V. M. Ustinov and A. E. Zhukov, Semicond. Sci. Technol. **15**, R41 (2000).
[12] M. Peter, K. Winkler, M. Maier, N. Herres, J. Wagner, D. Fekete, K. Bachem, and D. Richards, Appl. Phys. Lett. **67**, 2639 (1995).
[13] G. Ji, S. Agarwala, D. Huang, J. Chyi, and H. Morkoc, Phys. Rev. B **38**, 10571 (1988).
[14] K. Nishi, T. Anan, and S. Sugou, Proceedings of 1999 IEEE Digest of the LEOS Summer Topical Meetings, Piscataway, NJ, (1999), pp. III 39–III 40.
[15] A. D. Prins, D. J. Dunstan, J. D. Lambkin, E. P. O'Reilly, A. R. Adams, R. Pritchard, W. S. Truscott, and K. E. Singer, Phys. Rev. B **47**, 2191 (1993).
[16] S. M. North, P. R. Briddon, M. A. Cusack, and M. Jaros, Phys. Rev. B **58**, 12601 (1998).
[17] C. G. Van de Walle, Phys. Rev. B **39**, 1871 (1989).
[18] M. E. Rubin, H. R. Blank, M. A. Chin, H. Kroemer, and V. Narayanamurti, Appl. Phys. Lett. **70**, 1590 (1997).
[19] G. Liu, S.-L. Chuang, and S.-H. Park, J. Appl. Phys. **88**, 5554 (2000).
[20] P. Christol, P. Bigenwald, A. Joullie, Y. Cuminal, A. N. Baranov, N. Bertru, and Y. Rouillard, IEE Proc.-J: Optoelectron. **146**, 3 (1999).
[21] J. E. Cunningham, M. Dinu, J. Shah, F. Quochi, D. Kilper, W. Y. Jan, M. D. Williams, A. Mills, and W. E. Henderson, J. Vac. Sci. Technol. B **19**, 1948 (2001).
[22] R. Kaspi and K. R. Evans, J. Cryst. Growth **175-176**, 838 (1997).
[23] Y.-H. Cho, T. J. Schmidt, S. Bidnyk, G. H. Gainer, J. J. Song, S. Keller, U. K. Mishra, and S. P. DenBaars, Phys. Rev. B **61**, 7571 (2000).
[24] M. Vening, D. J. Dunstan, and K. P. Homewood, Phys. Rev. B **48**, 2412 (1993).
[25] J. R. Botha and A. W. R. Leitch, Phys. Rev. B **50**, 18147 (1994).
[26] M. P. C. M. Krijn, Semicond. Sci. Technol. **6**, 27 (1991).
[27] *Landolt-Bornstein Numerical Data and Functional Relationships in Science and Technology*, edited by W. Martienssen (Springer, Berlin, 1974), Vol. III/13A.
[28] *Antimonide-Related Strained-Layer Heterostructures*, edited by M. O. Manasreh (Gordon and Breach, Harwood, 1997), Vol. 3.
[29] Y. J. Ding, J. V. D. Veliadis, and J. B. Khurgin, J. Appl. Phys. **75**, 1727 (1994).
[30] P. Blood, IEEE J. Quantum Electron. **36**, 354 (2000).
[31] W. W. Chow and H. C. Schneider, Appl. Phys. Lett. **78**, 4100 (2001).